Available online at www.sciencedirect.com
SCIENCE DIRECT®
International Journal of Heat and Mass Transfer 48 (2005) 3591–3603
International Journal of HEAT and MASS TRANSFER
www.elsevier.com/locate/ijhmt

Stability of an oscillatory shear flow in a differentially heated vertical channel

Y.C. Chen *

Department of Energy and Resources, National United University, Miaoli 360, Taiwan, ROC

Received 7 April 2004; received in revised form 4 March 2005
Available online 23 May 2005

Abstract

The linear stability of an oscillatory shear flow in a differentially heated vertical channel was investigated numerically for $Re = 1000$ and $Pr = 0.7$. The Galerkin method is used to solve the disturbance momentum and energy equations. The results show that the least stable disturbance could be three-dimensional for higher flow oscillation frequency and larger flow oscillation amplitude, while it is two-dimensional in the isothermal oscillatory and heated steady channel flows. The flow oscillation acts to stabilize the flow at moderate and high oscillation frequencies, where the degree of stabilization increases with the oscillation amplitude; but, it acts to destabilize the flow and the amount of destabilization increases with the oscillation amplitude at low oscillation frequency. It is shown from the balance of disturbance kinetic energy budget that shear production is responsible for the flow instability. For the 2-D wave initiated instability, almost all the shear production is generated during a very short time interval at low oscillation frequency, while it is generated during most of the time of a cycle for the 3-D disturbance.

Keywords: Linear stability; Oscillatory shear flow; Mixed convection

1. Introduction

The processes of momentum, heat and mass transports in oscillatory isothermal or non-isothermal flows in tubes, ducts and channels have a variety of applications ranging from electronic device cooling, heat exchanger, biomedical sciences, and other cases of practical interests. Kurzweg [2], Zhang and Kurzweg [1], Kurzweg and Zhao [3], Kaviany [4], and Kaviany and Reckker [5] studied the problem of enhanced axial heat transfer in viscous fluids subjected to sinusoidal oscillations in conduits. Their analytical and experimental results show that the axial heat transferred in such oscillating flows can be several orders of magnitude larger than that obtained by pure molecular conduction. Liao et al. [6] presented an exact solution for small oscillatory flow Reynolds numbers in a zero-mean oscillatory laminar channel flow with a uniformly heated wall to simulate the forced convection cooling of electronic components on printed circuit boards. It was found that a maximum heat transfer enhancement of the order of 200% over the steady-flow case is obtained at Wormersely number of 2.0. Faghri et al. [7] indicated that the effect of pulsations on the average heat transfer rate of laminar oscillatory flow in a pipe is the result of an interaction between the velocity and temperature pulsations. The

* Tel.: +886 37 381392; fax: +886 37 381237.
E-mail address: ycchen@nuu.edu.tw

0017-9310/$ - see front matter © 2005 Elsevier Ltd. All rights reserved.
doi:10.1016/j.ijheatmasstransfer.2005.03.010

Nomenclature

E_s, E_b, E_d disturbance kinetic energies, defined in Eq. (18)
$\vec{e}_x$ unit vector in the x direction
g gravitational acceleration
Gr Grashof number, $g\beta_T\Delta T^*_w(2L)^3/v^2$
L half-width of channel
p pressure
Pr Prandtl number
Re Reynolds number, U^*_0L/v
t time
T period
ΔT^*_w wall temperature difference
T^* dimensional temperature
T^*_m mean wall temperature
U_B velocity at laminar base state
U^*_0 centerline velocity of the steady laminar flow
u_{rms} root mean square streamwise perturbation velocity, defined in Eq. (30)
u, v, w flow velocity components
$\vec{V}$ fluid velocity
x, y, z coordinates

Greek symbols
α streamwise wavenumber
β spanwise wavenumber
β_r $=L/\delta$
β_T thermal expansion coefficient
δ Stokes-layer thickness, $\sqrt{2v/\Omega^*}$
Λ $=\Lambda/\beta_r^2$, see Eq. (8)
θ dimensionless temperature, $(T^* - T^*_m)/\Delta T^*_w$
θ_B temperature at laminar base state
Λ oscillatory pressure gradient amplitude
v fluid kinematic viscosity
ρ fluid density
σ disturbance growth rate
ω_1 critical wave frequency of steady flow
Ω oscillation frequency

Superscripts
$*$ dimensional quantity
$'$ infinitesimal disturbance
$\hat{}$ complex amplitude function of disturbance, defined in Eq. (14)

Subscript
B at laminar base state

heat transfer characteristics of pulsating flow in curved tube by Rabadi et al. [8] showed that the Nussult number varies widely during a cycle and the effect is greatest for small values of the frequency parameter.

In the stability analysis of two-dimensional disturbances for non-zero-mean channel flow induced by oscillatory pressure gradient, Grosch and Salwen [9] found that for small amplitudes of mean velocity oscillation the modulated flow tends to stabilize the flow. For larger amplitudes of oscillation the modulated flow tends to destabilize the flow. Von Kerczek [10] also studied the stability of two-dimensional waves for the oscillatory plane Poiseuille flow by perturbation analysis about the critical Reynolds number of 5772.22 (based on the centerline velocity and half-width of channel). It was found that the oscillatory flow is more stable than the steady flow for values of oscillation frequencies greater than about one tenth of the frequency of the steady flow neutral disturbance. At very high and low oscillation frequencies, oscillatory flow slightly destabilize the flow. These results hold for the values of the velocity amplitude ratio at least up to 0.25. He did not find any strongly unstable modes. Singer et al. [11] performed both linear stability and direct numerical simulation of the oscillatory plane channel flow. Their results for larger amplitudes of oscillation agree with those of Von Kerczek but disagree with those of Grosch and Salwen.

In the effects of oscillatory nature of boundary conditions on the onset of Rayleigh–Benard convection, Finucane and Kelly [12] first found both experimentally and analytically that the onset could be delayed by thermal modulation (heated sinusoidally from below) at relatively high frequencies. The stabilizations on the onset of Rayleigh–Benard or Marangoni convections by means of non-planar oscillatory flows, where two components of the basic flow in the horizontal plane which are out of phase, were proposed by Kelly [14], Kelly and Hu [13], and Or and Kelly [15]. They found that the degree of stabilization seems likely to be substantial, especially at large values of the Prandtl number. In the linear stability analysis of mixed convection in a differentially heated vertical channel without flow oscillation, Chen and Chung [16] showed that the least stable disturbance is two-dimensional disturbance. However, the linear instability only addresses the first stage of the transition process—the growth of the linear waves propagating in the streamwise direction. When the linear wave amplitude exceeds a certain threshold, the non-linear interactions between waves arise. The flow transition

phenomena of mixed convection in the vertical channel flow were examined by Chen and Chung [17,18]. For a flow configuration in a differentially heated vertical channel, it is desired to know flow oscillation effects on the flow stability characteristics. Thus the linear stability analysis was investigated in this paper.

2. Formulation

The problem under investigation is the oscillatory heated shear flow, which is driven by both the imposed oscillatory pressure gradient and the buoyancy force, between two parallel long vertical plates separated by a distance, $2L$. A schematic of this system is given in Fig. 1. The gravitational force is aligned in the negative x-direction. The two vertical plates are kept at fixed temperatures of T_1^* and T_2^*, respectively. The dimensionless governing equations for continuity, momentum and energy can be written as:

$$\nabla \cdot \vec{V} = 0 \tag{1}$$

$$\frac{\partial \vec{V}}{\partial t} + (\vec{V} \cdot \nabla)\vec{V} = -\nabla p + \frac{Gr}{8Re^2}\theta \vec{e}_x + \frac{1}{Re}\nabla^2 \vec{V} \tag{2}$$

$$\frac{\partial \theta}{\partial t} + (\vec{V} \cdot \nabla)\theta = \frac{1}{RePr}\nabla^2 \theta \tag{3}$$

In the above equations, the coordinates are non-dimensionlized by the half-width of channel, L, the velocity ($\vec{V}$) by the centerline velocity of the steady laminar base flow, U_0^*, the pressure (p) by ρU_0^{*2}, and the time (t) by L/U_0^*. The parameters of $Re = U_0^* L/\nu$ is the Reynolds number, Pr is the Prandtl number, and $Gr = g\beta_T \Delta T_w^* (2L)^3/\nu^2$ is the Grashof number, where $\Delta T_w^* = T_2^* - T_1^*$ is the wall temperature difference. The Boussinesq approximation is used here, and viscous dissipation is neglected. Here $\theta = (T^* - T_m^*)/\Delta T_w^*$ is the dimensionless temperature, where T^* is the instantaneous fluid temperature, and T_m^* is the mean wall temperature.

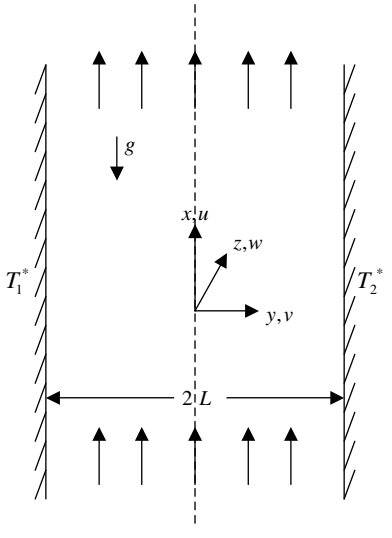

Fig. 1. The schematic of geometry and coordinate system ($T_2^* > T_1^*$).

2.1. Laminar base flow

The base flow is fully developed laminar flow, which are functions of y and t. The dimensionless imposed oscillatory pressure gradient at base laminar flow is expressed as the following:

$$-\frac{\partial p_B}{\partial x} = \frac{2}{Re}(1 + \Lambda \cos \Omega t) \tag{4}$$

where $\Omega = \Omega^* L/U_0^*$ is the dimensionless oscillation frequency of the imposed pressure gradient, and Ω^* is the dimensional angular frequency. Here Λ is the amplitude of the oscillatory pressure gradient. In the laminar base flow, the above governing equations (2) and (3) can be reduced to

$$\frac{\partial U_B}{\partial t} = -\frac{\partial p_B}{\partial x} + \frac{1}{Re}\frac{\partial^2 U_B}{\partial y^2} + \frac{Gr}{8Re^2}\theta_B \tag{5}$$

$$\frac{\partial^2 \theta_B}{\partial y^2} = 0 \tag{6}$$

where U_B and $\theta_B = (T_B^* - T_m^*)/\Delta T_w^*$ are the velocity and the temperature, respectively, of the laminar base flow. The associated boundary conditions are

$$\theta_B(-1,t) = -1/2, \quad \theta_B(1,t) = 1/2,$$
$$U_B(-1,t) = 0, \quad U_B(1,t) = 0 \tag{7}$$

The solutions of Eqs. (5)–(7) can be derived as the following:

$$U_B = 1 - y^2 + \frac{Gr}{96Re}(y - y^3) + \Lambda \Re\left\{\left[\frac{\cosh \beta_r(1+i)y}{\cosh \beta_r(1+i)} - 1\right] i e^{i\Omega t}\right\} \tag{8}$$

$$\theta_B = y/2 \tag{9}$$

where $i = \sqrt{-1}$ and $\Re$ denote the real part of the expression inside the braces. Here $\beta_r = L/\delta = \sqrt{\Omega Re/2}$ is the ratio of the half-width of channel to Stokes-layer thickness, δ, being defined as $\delta = \sqrt{2\nu/\Omega^*}$. In Eq. (8), Λ is equal to Λ/β_r^2, which is considered as the ratio of the amplitudes of the oscillatory to steady velocity in the isothermal oscillatory flow [10,11]. Fig. 2 plots the laminar base velocity profiles (U_B's) at various times of $t = T/8$, $T/4$, $T/2$, $3T/4$, $7T/8$, and T for $Re = 1000$, $\Omega/\omega_1 = 0.0503$, $Gr/Re = 76.21$, and $\Lambda = 0.2$, which

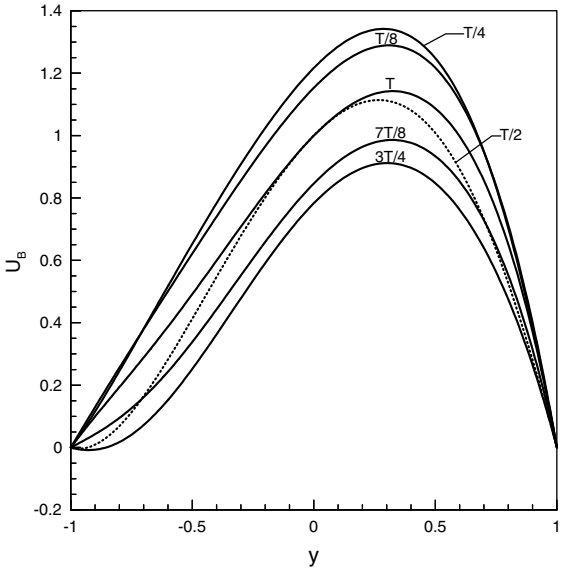

Fig. 2. The laminar base velocity profiles at some specific times for $Re = 1000$, $\Omega/\omega_1 = 0.0503$, $Gr/Re = 76.21$, and $\Delta = 0.2$.

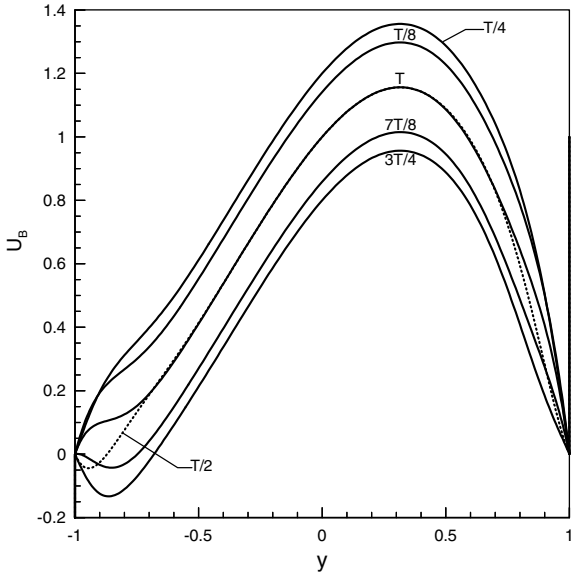

Fig. 3. The laminar base velocity profiles at some specific times for $Re = 1000$, $\Omega/\omega_1 = 0.503$, $Gr/Re = 86.45$, and $\Delta = 0.2$.

represents a point at the neutral stability boundary on the (Ω/ω_1, Gr/Re)-plane, as shown later in Fig. 4. Here $T = 2\pi/\Omega$ is the period of the imposed pressure gradient, and ω_1 is the critical wave frequency of the differentially heated steady channel flow, and its value is 0.3977 for $Re = 1000$, $Gr/Re = 79.7$, and $Pr = 0.7$ [16]. It is noted that the Reynolds number in Ref. [16] is based on the average velocity of laminar flow, not the centerline velocity. Fig. 2 shows that the velocity profile is not symmetric due to the differentially heated walls. The location of the peak value of each velocity curve is close to the side of the hotter wall of $y = 1$. The peak value of U_B at $t = 0.24T$ (close to the curve of $t = T/4$ in Fig. 2) is about 1.34, which is the largest during a cycle. The smallest peak value of U_B is about 0.9, which occurs at $t = 0.74T$ (close to the curve of $t = 3T/4$), that is, the U_B decays during half of the period from $t = 0.24T$ to $t = 0.74T$ and grows during other half of the period. Fig. 2 demonstrates that the variation of the velocity is substantial during a cycle. There are reverse flows near the cooler wall of $y = -1$ at curves of $t = T/2$ and $3T/4$.

At higher oscillation frequency and Grashof number for $\Omega/\omega_1 = 0.503$, $Gr/Re = 86.45$, and $\Delta = 0.2$, Fig. 3 shows that the velocity profile near the cooler wall of $y = -1$ is severely distorted and a wide range of reverse flow is seen during some time interval of a cycle. The variation of velocity near the cooler wall during a cycle is also larger than that in Fig. 2. As compared to the isothermal oscillatory channel flow (see Fig. 1 in the paper of Singer et al. [11]), the range of the reverse flow in Fig. 3 is much wider and the value of U_B at $y = -0.864$ is as low as -0.133 for $t = 3T/4$. The largest of the peak value of U_B occurs at $t = T/4$, which is almost the same as that in Fig. 2.

2.2. Linear stability analysis

In the linear stability analysis, infinitesimal disturbances are imposed on the laminar base flow, thus the velocity, pressure, and temperature fields can be written as

$$\vec{V} = U_B(y,t)\vec{e}_x + \vec{V}', \quad p = p_B(y,t) + p', \\ \theta = \theta_B(y,t) + \theta' \tag{10}$$

where the prime denotes an infinitesimal disturbance. By substituting Eq. (10) into (1)–(3) and neglecting the higher-order terms, the linearized continuity, momentum, and energy equations for the perturbed quantities become the following:

$$\nabla \cdot \vec{V}' = 0 \tag{11}$$

$$\frac{\partial \vec{V}'}{\partial t} + (\vec{V}' \cdot \nabla)\vec{U}_B + (\vec{U}_B \cdot \nabla)\vec{V}' \\ = -\nabla p' + \frac{Gr}{8Re^2}\theta'\vec{e}_x + \frac{1}{Re}\nabla^2\vec{V}' \tag{12}$$

$$\frac{\partial \theta'}{\partial t} + U_B\frac{\partial \theta'}{\partial x} + v'\frac{\partial \theta_B}{\partial y} = \frac{1}{RePr}\nabla^2\theta' \tag{13}$$

where $\vec{U}_B = U_B\vec{e}_x$, the disturbances of the velocity, pressure, and temperature, assume the following normal mode forms, respectively:

$$\vec{V}' = \hat{\vec{V}}(y,t)e^{i(\alpha x+\beta z)}, \quad p' = \hat{p}(y,t)e^{i(\alpha x+\beta z)}, \quad \theta' = \hat{\theta}(y,t)e^{i(\alpha x+\beta z)} \tag{14}$$

where $\hat{\vec{V}} = (\hat{u},\hat{v},\hat{w})$ with $\hat{u}$, $\hat{v}$, and $\hat{w}$ are the velocity components in the x-, y-, and z-directions, respectively. Here α and β are the wavenumbers in the streamwise and spanwise directions, respectively. By substituting Eq. (14) into (11)–(13) and eliminating the pressure term, the linearized momentum and energy equations are as follows:

$$\frac{\partial}{\partial t}\left[\frac{\partial^2\hat{v}}{\partial y^2}-(\alpha^2+\beta^2)\hat{v}\right] = \frac{1}{Re}\left[\frac{\partial^4\hat{v}}{\partial y^4}-2(\alpha^2+\beta^2)\frac{\partial^2\hat{v}}{\partial y^2}+(\alpha^2+\beta^2)^2\hat{v}\right] - i\alpha\frac{Gr}{8Re^2}\frac{\partial\hat{\theta}}{\partial y} - i\alpha\left\{U_B\frac{\partial^2\hat{v}}{\partial y^2}-\left[\frac{\partial^2 U_B}{\partial y^2}+(\alpha^2+\beta^2)U_B\right]\hat{v}\right\} \tag{15}$$

$$\frac{\partial\hat{\theta}}{\partial t} = \frac{1}{RePr}\left[\frac{\partial^2\hat{\theta}}{\partial y^2}-(\alpha^2+\beta^2)\hat{\theta}\right] - i\alpha U_B\hat{\theta} - \frac{\partial\theta_B}{\partial y}\hat{v} \tag{16}$$

The associated boundary conditions for non-permeable rigid walls with fixed but different wall temperatures are

$$\hat{v} = \frac{\partial\hat{v}}{\partial y} = \hat{\theta} = 0, \quad \text{at } y = \pm 1 \tag{17}$$

Eqs. (15) and (16) and the corresponding boundary conditions constitute an eigenvalue problem.

2.3. Energy budget analysis

To understand the driving mechanisms of flow instability, it is necessary to keep track of the balance of the disturbance kinetic energy budget, E_k, which is written as [19,20]

$$\frac{d}{dt}\langle(u'^2+v'^2+w'^2)/2\rangle = -\left\langle u'v'\frac{\partial U_B}{\partial y}\right\rangle + \frac{Gr}{8Re^2}\langle u'\theta'\rangle - \frac{1}{Re}\langle(\nabla u')^2+(\nabla v')^2+(\nabla w')^2\rangle = E_s+E_b+E_d \tag{18}$$

where the bracket $\langle\ \rangle$ denotes the integration over the volume of the disturbance wave. The first term on the right-hand side of Eq. (18) represents the kinetic energy production by shear, E_s, which is the product of the Reynolds shear stress and flow strain rate. The second term represents the buoyant production, E_b, which is absent in the isothermal flow. The third term represents the energy dissipation, E_d, which is through molecular viscosity. On the neutral stability curve, the net growth or decay of the disturbances over a cycle is zero. The velocity disturbance v' is directly obtained from Eq. (15). To obtain the velocity disturbances u' and w', the additional linearized equation, as shown in following, has to be solved.

$$\frac{\partial\hat{\eta}}{\partial t} = -i\alpha U_B\hat{\eta} - \beta\frac{\partial U_B}{\partial y}\hat{v} + \frac{1}{Re}\left[\frac{\partial^2\hat{\eta}}{\partial y^2}-(\alpha^2+\beta^2)\hat{\eta}\right] + \beta\frac{Gr}{8Re^2}\hat{\theta} \tag{19}$$

where $\hat{\eta} = \beta\hat{u} - \alpha\hat{w}$ and the associated boundary condition for Eq. (19) is $\hat{\eta}(y\pm 1,t) = 0$. By using the linearized continuity equation, $\hat{u}$ and $\hat{w}$ can be written in terms of $\hat{v}$ and $\hat{\eta}$ as

$$\hat{u} = \frac{1}{\alpha^2+\beta^2}\left(i\alpha\frac{\partial\hat{v}}{\partial y}+\beta\hat{\eta}\right) \tag{20}$$

$$\hat{w} = \frac{1}{\alpha}(\beta\hat{u}-\hat{\eta}) = \frac{1}{\alpha}\left[\frac{\beta}{\alpha^2+\beta^2}\left(i\alpha\frac{\partial\hat{v}}{\partial y}+\beta\hat{\eta}\right)-\hat{\eta}\right] \tag{21}$$

2.4. Numerical method

The Galerkin method is used to solve Eqs. (15) and (16) and their associated boundary conditions (including Eq. (19) in the energy budget calculation). In this method, the test (weighted) functions are the same as the base (trial) functions. Thus the $\hat{v}$, $\hat{\theta}$, and $\hat{\eta}$ are expanded in the following forms:

$$\hat{v} = \sum_{n=0}^{N} b_n(t)\xi_n(y) \tag{22a}$$

$$\hat{\theta} = \sum_{n=0}^{N} c_n(t)\phi_n(y) \tag{22b}$$

$$\hat{\eta} = \sum_{n=0}^{N} d_n(t)\phi_n(y) \tag{22c}$$

where $b_n(t)$, $c_n(t)$ and $d_n(t)$ are the unknown coefficients. We adopt the base functions proposed by Singer et al. [11] for $\hat{v}$. The base functions for $\hat{\theta}$ and $\hat{\eta}$ have slightly different form [16]. They are

$$\xi_n(y) = (1-y^2)^2P_n(y) \tag{23a}$$

$$\phi_n(y) = (1-y^2)P_n(y) \tag{23b}$$

where each base function $\xi_n(y)$ or $\phi_n(y)$ satisfies the boundary conditions and $P_n(y)$ is the Legendre polynomial of order n. Legendre polynomials could provide good resolution near the wall [21] which is essential for the computation of flow driven by the imposed oscillatory pressure gradient. By following the similar steps outlined by Chen and Chung [20], the governing equations (15) and (16) become

$$\boldsymbol{R}\frac{d\boldsymbol{a}}{dt} = \boldsymbol{S}\boldsymbol{a} + \boldsymbol{O}\boldsymbol{a} \tag{24a}$$

$$\boldsymbol{a} = \begin{pmatrix} \{b\} \\ \{c\} \end{pmatrix}, \quad \boldsymbol{R} = \begin{pmatrix} [D] & [0] \\ [0] & [H] \end{pmatrix},$$
$$\boldsymbol{S} = \begin{pmatrix} [E] & [G] \\ [K] & [I] \end{pmatrix}, \quad \boldsymbol{O} = \begin{pmatrix} [F] & [0] \\ [0] & [J] \end{pmatrix} \tag{24b}$$

where the vector $\boldsymbol{a}$ is composed of the unknown coefficient $b_n(t)$ and $c_n(t)$. The elements in Eq. (24b) are

$$D_{m,n} = -\int_{-1}^{1} [\xi'_m \xi'_n + (\alpha^2+\beta^2)\xi_m \xi_n] \mathrm{d}y \tag{25a}$$

$$E_{m,n} = \frac{1}{Re}\int_{-1}^{1} [\xi''_m \xi''_n + 2(\alpha^2+\beta^2)\xi'_m \xi'_n + (\alpha^2+\beta^2)^2 \xi_m \xi_n] \mathrm{d}y \tag{25b}$$

$$F_{m,n} = \mathrm{i}\alpha \int_{-1}^{1} \{[U''_{\mathrm{B}} + (\alpha^2+\beta^2)U_{\mathrm{B}}]\xi_m \xi_n - U_{\mathrm{B}} \xi_m \xi''_n\} \mathrm{d}y \tag{25c}$$

$$G_{m,n} = -\mathrm{i}\alpha \frac{Gr}{8Re^2}\int_{-1}^{1} \xi_m \phi'_n \mathrm{d}y \tag{25d}$$

$$H_{m,n} = \int_{-1}^{1} \phi_m \phi_n \mathrm{d}y \tag{25e}$$

$$I_{m,n} = -\frac{1}{RePr}\int_{-1}^{1} [\phi'_m \phi'_n + (\alpha^2+\beta^2)\phi_m \phi_n] \mathrm{d}y \tag{25f}$$

$$J_{m,n} = -\mathrm{i}\alpha \int_{-1}^{1} U_{\mathrm{B}} \phi_m \phi_n \mathrm{d}y \tag{25g}$$

$$K_{m,n} = -\int_{-1}^{1} \theta'_{\mathrm{B}} \phi_m \xi_n \mathrm{d}y \tag{25h}$$

Lobatto quadrature is used to compute the matrice which involve the unsteady base velocity and its derivative. Other matrices are evaluated by using the orthogonality properties of Legendre polynomials [20]. Following the same solution procedure employed by Singer et al. [11], a generalization of Eq. (24) is written as

$$\boldsymbol{R}\frac{\mathrm{d}\boldsymbol{A}}{\mathrm{d}t} = \boldsymbol{S}\boldsymbol{A} + \boldsymbol{O}\boldsymbol{A} \tag{26}$$

where $\boldsymbol{A}$ is a matrix of solution vector and it has the form

$$\boldsymbol{A}(t) = \boldsymbol{P}(t)\exp(t\boldsymbol{Q}) \tag{27}$$

where $\boldsymbol{Q}$ is a constant matrix, $\boldsymbol{P}$ is a non-singular periodic matrix and its period, T, is the same as that of $\boldsymbol{O}$ and is imposed by the pressure gradient. Crank–Nicolson scheme is chosen for the discretization in time. Generally, using 250 time steps per cycle are enough to give results that were indistinguishable from those using higher time steps. Number of time steps was increased for the computing at very low oscillation frequency.

Table 1
The effect of the number of the Legendre polynomials on the growth rate of the disturbance for $Re = 1000$, $Pr = 0.7$, $Gr/Re = 94.44$, $\Omega/\omega_1 = 0.265$, $\Delta = 0.2$, $\alpha = 1.003$, $\beta = 0$

N	Growth rate (σ)
21	−0.00007817357
31	0.00000151262
41	0.00000151188
51	0.00000151188
61	0.00000151188
71	0.00000151188

The complete set of solution can be captured by initializing $\boldsymbol{A}$ to the identity matrix.

$$\boldsymbol{A}(0) = \boldsymbol{I} = \boldsymbol{P}(0)\exp(0\boldsymbol{Q}) \tag{28a}$$

thus

$$\boldsymbol{P}(0) = \boldsymbol{I} \tag{28b}$$

At the end of a period,

$$\boldsymbol{A}(T) = \boldsymbol{P}(T)\exp(T\boldsymbol{Q}) = \boldsymbol{P}(0)\exp(T\boldsymbol{Q}) = \exp(T\boldsymbol{Q}) \tag{28c}$$

If the eigenvalues of $\boldsymbol{A}(T)$ are λ_j, the associated growth rates, σ_j, are

$$\sigma_j = \frac{\ln(\lambda_j)}{T} \tag{29}$$

The flow is stable, neutrally stable, or unstable when the value of the real part of σ_j is positive, zero, or negative, respectively. Galerkin method is also used to solve governing equations of (15), (16), and (19) for the energy budget analysis. We had applied above solution method to linear stability of an oscillatory two-phase channel flow [22]. The effect of the number of the Legendre polynomials on the growth rate for higher Grashof number (with larger distortion of velocity profile) has been tested. As shown in Table 1, the growth rate changes very small for $N \geqslant 51$. Same results are also obtained for some other cases. Therefore $N = 51$ is used in all the computations. In the code verification, our isothermal oscillatory plane channel flow results, as shown in Table 2, agree well with those given by Singer et al. [11] and Von Kerczek [10].

3. Results and discussion

The parameters of $Re = 1000$ and $Pr = 0.7$ were used in these calculations. Fig. 4 demonstrates the neutral stability boundaries on the (Ω/ω_1,Gr/Re)-plane for the two-dimensional (solid line) and three-dimensional (dashed line) disturbances initiated instabilities for oscillation amplitude, $\Delta = 0.2$, where $\omega_1 = 0.3977$ [16]. It is seen from Fig. 4 that the two-dimensional wave (with zero

Table 2
Comparison of growth rates of an isothermal oscillatory channel flow for $Re = 5772.22$, $\alpha = 1.0206$, $\beta = 0$, $\omega_1 = 0.2694$

Ω	Δ	Von Kerczek	Singer et al.		Our results
			Linear	Full simulation	
$\omega_1/22$	0.20	$+5.0\times10^{-3}$	$+5.6\times10^{-3}$	$+4.8\times10^{-3}$	$+4.8\times10^{-3}$
$\omega_1/7$	0.20	-8.0×10^{-3}	-7.7×10^{-3}	-8.2×10^{-3}	-8.2×10^{-3}
$\omega_1/3$	0.05	-2.2×10^{-3}	-2.2×10^{-3}	-2.2×10^{-3}	-2.2×10^{-3}
$\omega_1/3$	0.20	-2.6×10^{-2}	-2.7×10^{-2}	-2.7×10^{-2}	-2.7×10^{-2}
ω_1	0.10	-1.0×10^{-3}	-1.0×10^{-3}	-1.1×10^{-3}	-1.0×10^{-3}
ω_1	0.25	-5.5×10^{-3}	-5.3×10^{-3}	-5.3×10^{-3}	-5.3×10^{-3}
$2\omega_1$	0.20	-4.1×10^{-4}	-5.7×10^{-4}	-5.7×10^{-4}	-5.7×10^{-4}
$4\omega_1$	0.20	-5.1×10^{-5}	-4.3×10^{-5}	-5.2×10^{-5}	-5.1×10^{-5}
$16\omega_1$	0.20	$+4.6\times10^{-9}$	$+4.6\times10^{-5}$	-3.9×10^{-6}	$+4.6\times10^{-7}$

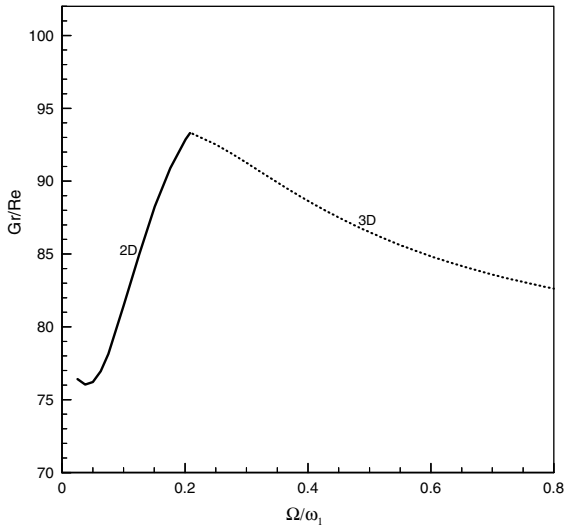

Fig. 4. The neutral stability boundaries on the (Ω/ω_1, Gr/Re)-plane for $Re = 1000$ and $\Delta = 0.2$.

spanwise wavenumber) is the least stable mode for flow oscillation frequency less than 0.21. The critical value of $(Gr/Re)_c$ for the 2-D disturbance changes little for Ω/ω_1 between 0.025 and 0.07, then it increases rapidly with the oscillation frequency until it reaches a peak value at about $\Omega/\omega_1 \approx 0.21$, where the three-dimensional disturbance becomes the least stable mode. After that, it falls down and the $(Gr/Re)_c$ decreases with increasing Ω/ω_1, but its decreasing rate is slower. All the least stable modes for $0.21 < \Omega/\omega_1 < 0.8$ are three-dimensional. This indicates that for higher flow oscillation frequency the three-dimensional instability initiates in the primary instability stage, while in the isothermal oscillatory channel flow and the differentially heated steady channel flow, the instability starts with 2-D wave, and the 3-D behavior initiates only after the 2-D waves reach finite amplitudes. The $(Gr/Re)_c$ for the differentially heated non-oscillatory channel flow is 79.7 for $Re = 1000$ and $Pr = 0.7$ [16]. Fig. 4 shows that the effect of flow oscillation destabilizes the flow for oscillation frequency of $\Omega/\omega_1 < 0.09$, but it begins to stabilizes the flow for Ω/ω_1 between 0.09 and 0.8. This indicates that the effect of flow oscillation stabilizes the flow except at low oscillation frequency.

Next Fig. 5 plots the variations of the critical wavenumbers of 2-D and 3-D disturbances with the flow oscillation frequency along the neutrally stable curve for $\Delta = 0.2$. For the two-dimensional wave initiated instability, the critical streamwise wavenumber, α_c, changes very slightly with the oscillation frequency. All the α_c's are close to that (=1.02) of the two-dimensional Tollmien–Schlichting (T–S) wave for the isothermal non-oscillatory plane channel flow [23]. At

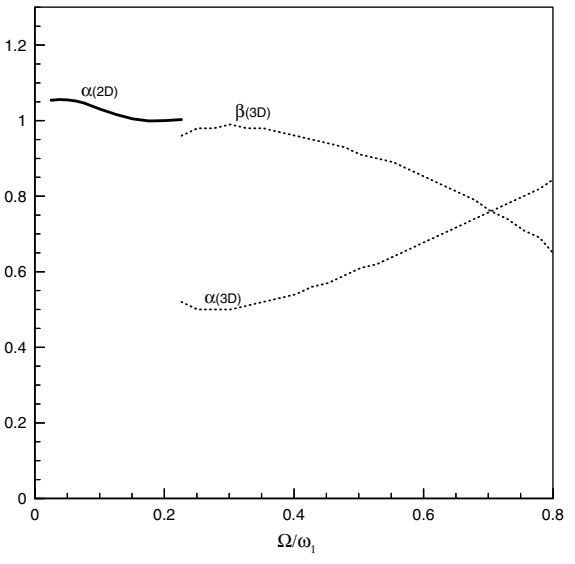

Fig. 5. The variations of the critical streamwise wavenumber, α_c, and the critical spanwise wavenumber, β_c, with the flow oscillation frequency Ω/ω_1 along the neutral stability curve for $Re = 1000$ and $\Delta = 0.2$.

$\Omega/\omega_1 \approx 0.21$, the least stable disturbance becomes three-dimensional, and the α_c abruptly reduced to 0.52, which is nearly half of that of the two-dimensional wave at $\Omega/\omega_1 = 0.201$. For the 3-D disturbance, the variations of the α_c and the β_c, with the oscillation frequency are small for Ω/ω_1 between 0.21 and 0.38. After that, the trend of α_c and β_c is different, the α_c increases, but β_c decreases with further increase of Ω/ω_1.

The effects of the oscillation amplitude, Δ, on the stability characteristics are shown in Table 3. At a low oscillation frequency of $\Omega/\omega_1 = 0.0754$, all the values of $(Gr/Re)_c$'s are smaller than that (79.7) of the differentially heated steady channel flow, that is, the flow oscillation acts to destabilize the flow. It is also seen that the degree of destabilization increases with oscillation amplitude at $\Omega/\omega_1 = 0.0754$. Table 3 also demonstrates that all the instabilities are initiated by the two-dimensional waves at $\Omega/\omega_1 = 0.0754$. The variation of the α_c with oscillation amplitude for 2-D wave is very small, they are very close to that (=1.02) of the isothermal non-oscillatory plane channel flow.

The oscillation amplitude effect on the stability characteristic has a substantial change at the moderate oscillation frequency of $\Omega/\omega_1 = 0.226$. The least stable mode is the 2-D wave for $\Delta \leqslant 0.15$, while it switches to three-dimensional disturbance for $\Delta \geqslant 0.2$. This indicates that the least stable mode tends to become three-dimensional at higher oscillation amplitudes. The effect of the oscillation amplitude on the $(Gr/Re)_c$ at $\Omega/\omega_1 = 0.226$ is totally different from that at $\Omega/\omega_1 = 0.0754$. All the $(Gr/Re)_c$'s are larger than 79.7, that is, the flow oscillation acts to stabilize the flow, and the amount of stabilization increases with oscillation amplitude. The α_c's for the 2-D waves at $\Omega/\omega_1 = 0.226$ are also very close to 1.02 of the T–S wave. When the least stable mode switches to the three-dimensional disturbance at $\Delta = 0.2$, the α_c is abruptly reduced to a value of 0.52, which is about half of that of the T–S wave. The α_c for $\Delta \geqslant 0.2$ decreases with increasing oscillation amplitude.

Table 3
The effects of the oscillation amplitude (Δ) on the critical values of Gr/Re and the critical wavenumbers of α_c and β_c along the neutrally stable curve at three specify oscillation frequencies for $Re = 1000$ and $\Delta = 0.05$, 0.1, 0.15, 0.2, 0.25, and 0.3

Ω/ω_1	Δ	$(Gr/Re)_c$	α_c	β_c	Mode
0.0754	0.05	79.6	1.04	0	2-D
	0.10	79.3	1.04	0	2-D
	0.15	78.8	1.04	0	2-D
	0.20	78.2	1.05	0	2-D
	0.25	77.6	1.05	0	2-D
	0.30	76.9	1.06	0	2-D
0.226	0.05	80.7	1.04	0	2-D
	0.10	83.6	1.03	0	2-D
	0.15	88.3	1.02	0	2-D
	0.20	93.0	0.52	0.96	3-D
	0.25	96.8	0.42	1.02	3-D
	0.30	100.2	0.36	1.05	3-D
0.503	0.05	80.6	1.04	0	2-D
	0.10	82.9	0.88	0.59	3-D
	0.15	84.8	0.68	0.85	3-D
	0.20	86.5	0.61	0.91	3-D
	0.25	87.9	0.56	0.95	3-D
	0.30	89.2	0.52	0.98	3-D

At higher oscillation frequency of $\Omega/\omega_1 = 0.503$, the instability is initiated by the 2-D wave only at the low oscillation amplitude of $\Delta = 0.05$, and its α_c is also very close to that of T–S wave. The least stable mode quickly switches to the three-dimensional at $\Delta = 0.1$. This shows that at moderate and high oscillation frequencies, the least stable disturbances tend to become three-dimensional when the oscillation amplitude exceeds a threshold value. This threshold value is lower when the oscillation frequency is higher. It is also seen that all the $(Gr/Re)_c$'s are larger than 79.7 and the amount of stabilization increases with oscillation amplitude at $\Omega/\omega_1 = 0.503$. For 3-D disturbance, Table 3 shows that the α_c decreases, but the β_c increases with the oscillation amplitude. This behavior is different from the effect of oscillation frequency on the wavenumbers, where generally the α_c increases, but β_c decreases with increasing oscillation frequency, as shown earlier in Fig. 5.

The variation of the root mean square streamwise perturbation velocity during a cycle may provide information on the disturbance development. Some discussions on the r.m.s. streamwise velocity characteristics for the isothermal oscillatory channel flow can be found in Singer et. al. [11]. It is defined by

$$u_{\mathrm{rms}}(y,t) = \sqrt{\hat{u}(y,t)^2} \tag{30}$$

For the instability initiated by the 2-D wave, the r.m.s. streamwise perturbation velocity profiles at various times for $Re = 1000$, $\Omega/\omega_1 = 0.0503$, $\Delta = 0.2$, $Gr/Re = 76.21$, and $\alpha = 1.055$, are plotted in Fig. 6(a)–(h). It is seen that the variation of the amplitude of u_{rms} during a cycle is large. The amplitudes of u_{rms}'s from Fig. 6(a)–(e) are very small (note the large changes in the scale of the ordinate in Fig. 6(e)–(h)). The u_{rms} grows rapidly at $t = 3T/4$, and reaches the peak value at $t = 7T/8$ in Fig. 6(g). After that it decays very quickly. Fig. 6(a)–(h) also shows that the profiles of u_{rms}'s are not symmetric, while they are symmetric to the channel center (see Figs. 3 and 7 in the paper of Singer et al. [11]) for the isothermal oscillatory shear flow. As pointed out by Singer et al. [11], the existence of double peak structure is an indication that there is an energy exchange between the base flow and the two-dimensional wave in the region between the peaks. The u_{rms}'s in Fig. 6(f)–(h) also have double peak structures. This shows that the energy exchange between the base flow and the waves is strong

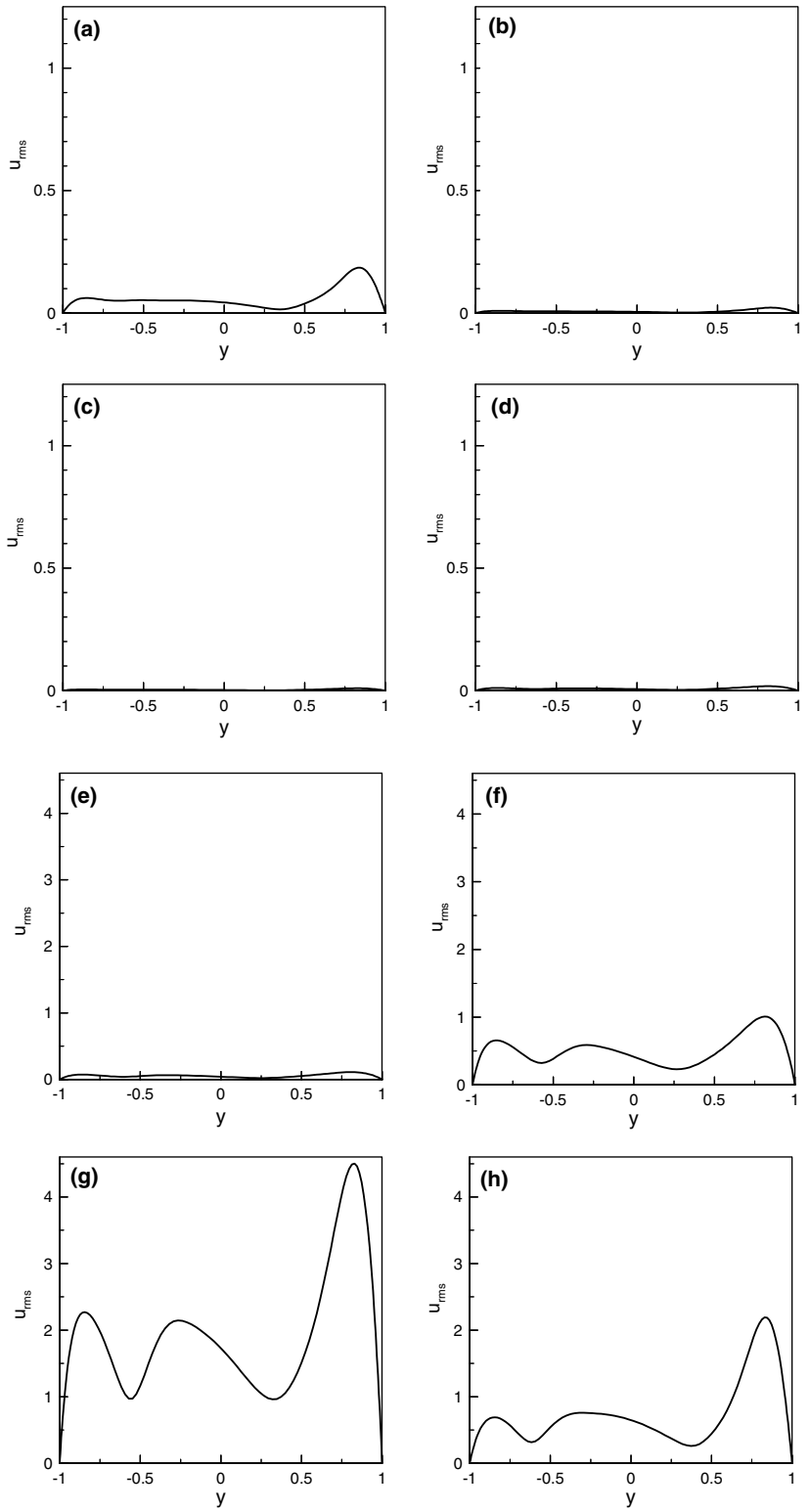

Fig. 6. The root mean square streamwise perturbation velocity profiles for $\Omega/\omega_1 = 0.0503$, $Re = 1000$, $Gr/Re = 76.21$, $\Delta = 0.2$, $\alpha = 1.055$, and $\beta = 0$ at various times of (a) $T/8$, (b) $T/4$, (c) $3T/8$, (d) $T/2$, (e) $5T/8$, (f) $3T/4$, (g) $7T/8$, and (h) T.

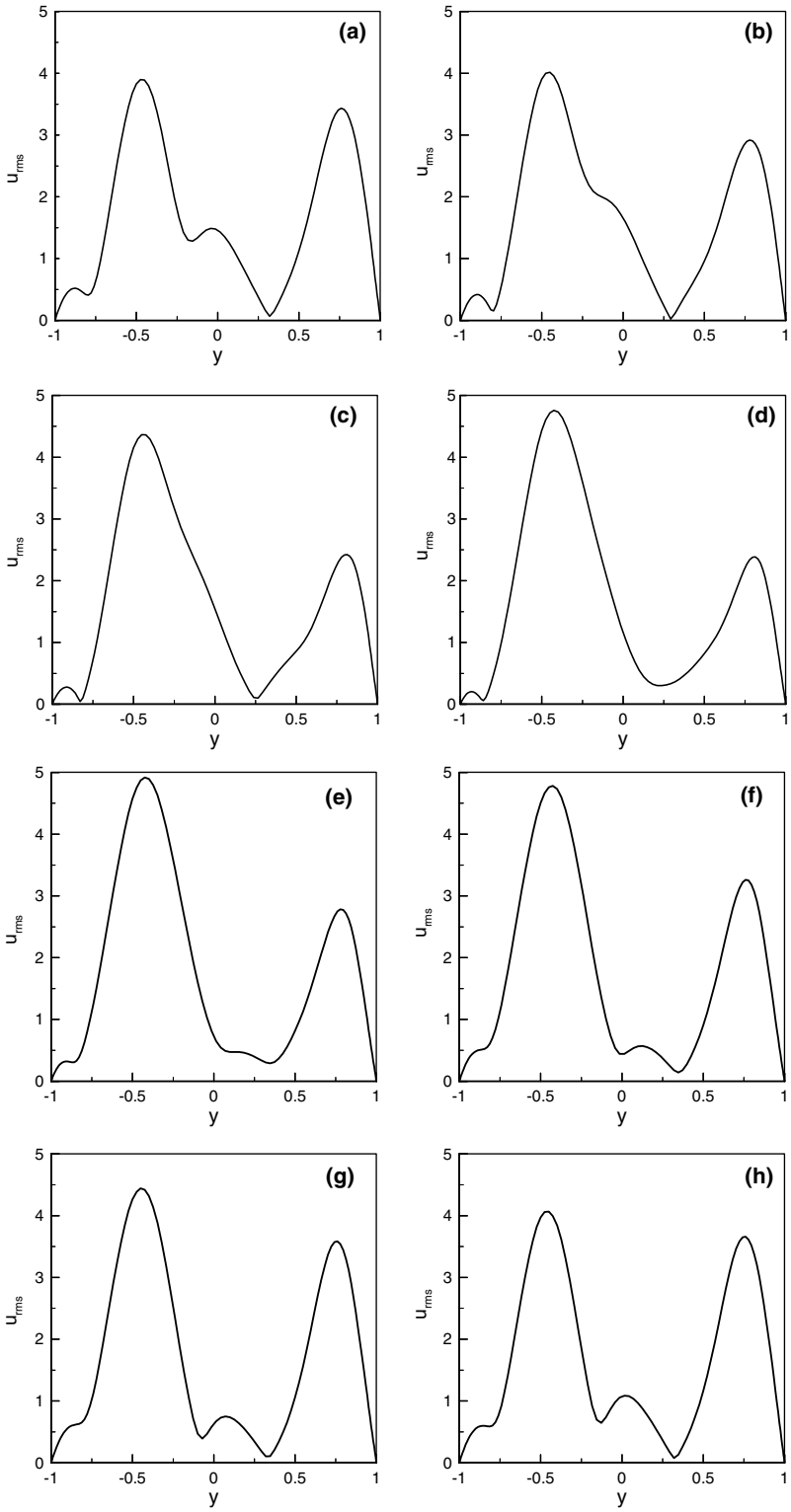

Fig. 7. The root mean square streamwise perturbation velocity profiles for $\Omega/\omega_1 = 0.503$, $Re = 1000$, $Gr/Re = 86.45$, $\Delta = 0.2$, $\alpha = 0.53$, and $\beta = 0.61$ at various times of (a) $T/8$, (b) $T/4$, (c) $3T/8$, (d) $T/2$, (e) $5T/8$, (f) $3T/4$, (g) $7T/8$, and (h) T.

during the time period between $t = 3T/4$ and T. The rapid increase of u_{rms} indicates that the disturbances strongly draw energy from the base flow. As shown before in Fig. 2, the base velocity of U_B grows during half of the period from its smallest value at $t = 0.74T$ to the largest value at $t = 1.24T$ (the velocity profile at $t = 1.24T$ is the same with that at $t = 0.24T$). This indicates that the growth of the disturbance mainly occurs during the early stage beginning when the U_B grows from its smallest value. It is noted that the locations of the peak value of u_{rms}'s in Fig. 6(a)–(h) are all near the hotter wall of $y = 1$, where the base velocities are large.

For the flow instability initiated by the 3-D disturbance, Fig. 7(a)–(h) plot the r.m.s. streamwise perturbation velocities for $\Omega/\omega_1 = 0.503$, $\Delta = 0.2$, $Gr/Re = 86.45$, $\alpha = 0.53$, and $\beta = 0.61$. It is worth noting that the locations of all the peak values of u_{rms}'s are located in the left-hand side of the channel between $y = 0$ and $y = -1$ (cooler wall), while they are located near the hotter wall for the 2-D disturbance. It is also seen that the amplitudes of u_{rms}'s in Fig. 7(a)–(h) are also large through the whole cycle, that is, its variation of the amplitude of u_{rms} during a cycle is much smaller than that in Fig. 6(a)–(h). All the profiles in Fig. 7(a)–(h) also have double peak structures. This indicates that the energy exchange between disturbances and the base flow for 3-D disturbance are generally strong through the cycle.

As indicated in Eq. (18), the development of the disturbance kinetic energy provides information on the driving mechanisms of flow instability. After one or two cycles, the disturbance kinetic energy profile becomes periodic and thus independent of the initial condition. For the two-dimensional wave at a low oscillation frequency of Ω/ω_1 =0.053, Fig. 8 presents the variation of each kinetic energy budget term with time for $Gr/Re = 76.21$, $\Delta = 0.2$, and $\alpha = 1.055$. It shows that the contribution of energy generation from the buoyant production, E_b, is negligible through the cycle. Thus the shear production, E_s, is responsible for the flow instability at $\Omega/\omega_1 = 0.053$. This type of instability is called thermal-shear instability, where the base velocity profile is distorted sufficiently to become unstable as a result of heating, but most of the kinetic energy for the instability comes from the shear production [20]. Such type instability also occurs for lower Prandtl number and higher Reynolds number for the steady heated vertical channel flow [16].

Fig. 8 shows that the shear production, E_s, rises sharply from a small value at about $t = 1.75T$ to a maximum value at about $t = 1.87T$. As time progresses, it falls down abruptly, and becomes near zero at about $t = 1.95T$. It is worth noting that the time interval for the kinetic energy generation by shear to initiate the flow instability occurs only at about 1/5 period of a cycle. The E_s is negligible or smaller than zero during the rest time of a cycle. This behavior reflects the characteristic of

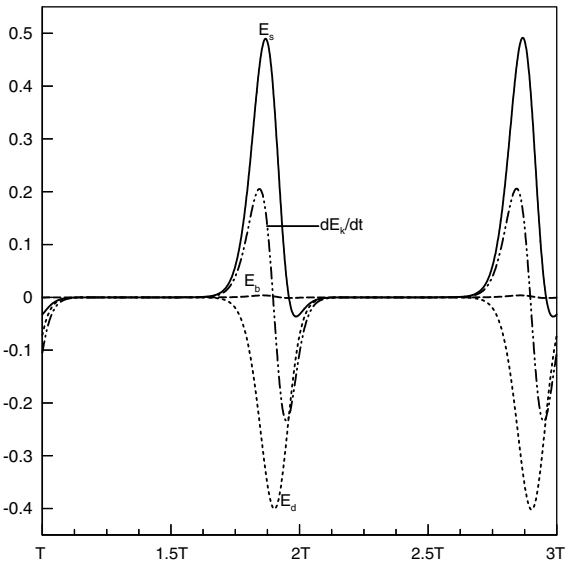

Fig. 8. The variation of each kinetic energy budget term with time for $\Omega/\omega_1 = 0.0503$, $Re = 1000$, $Gr/Re = 76.21$, $\Delta = 0.2$, $\alpha = 1.055$, and $\beta = 0$.

u_{rms}, where the u_{rms} also grows rapidly during a very short time interval, as shown in Fig. 6(a)–(h). It is also shown earlier in Fig. 2 that the base velocity begins to rise from its smallest value at $t = 1.74T$. This indicates that almost all of the kinetic energy is generated during the earlier stage when the base velocity begins to rise from its smallest value. Fig. 8 also shows that the rapid increase of E_s also induces the quick rising of the kinetic energy dissipation, E_d. The development process of E_d is basically similar to that of E_s, but it just lags behind E_s for a very short time period. The change rate of disturbance kinetic energy budget, dE_k/dt, is mainly dependent on E_s and E_d. Fig. 8 shows that it rises quickly with a maximum value at about $t = 1.85T$ and falls down quickly and becomes negative with a minimum value at about $t = 1.95T$.

For the flow instability initiated by the 3-D disturbance, Fig. 9 plots the variation of each kinetic energy budget term with time from for $\Omega/\omega_1 = 0.503$, $Gr/Re = 86.45$, $\Delta = 0.2$, $\alpha = 0.61$, and $\beta = 0.91$. The curve of E_s or dE_k/dt has double peaks during a cycle. The main difference of E_s between Figs. 8 and 9 is that the shear production is generated during most of the time of a cycle for the 3-D disturbance, while it is generated during only about 1/5 period of a cycle for the 2-D disturbance. The buoyant production in Fig. 9 is also negligible through the cycle. Thus it also belongs to thermal-shear instability at higher oscillation frequency. The kinetic energy dissipation, E_d, in Fig. 9 is more uniformly distributed through the whole cycle, while it is close to zero about 4/5 period of a cycle in Fig. 8. This characteristic of E_s in Fig. 9 also reflects the behavior

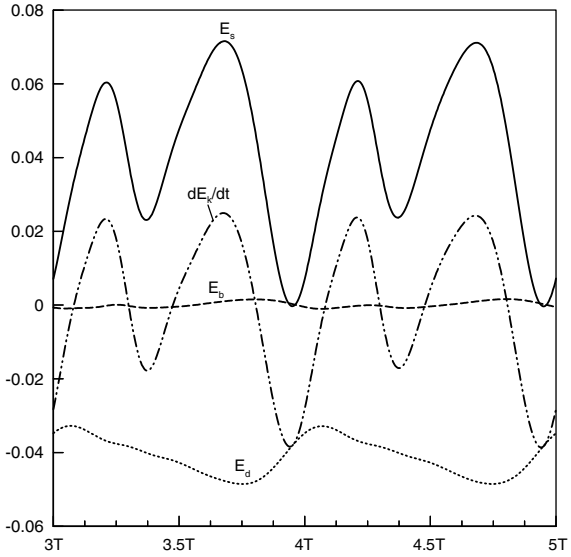

Fig. 9. The variation of each kinetic energy budget term with time for $\Omega/\omega_1 = 0.503$, $Re = 1000$, $Gr/Re = 86.45$, $\alpha = 0.53$, and $\beta = 0.61$.

of the u_{rms}. As shown earlier in Fig. 7, the u_{rms}'s are large and their amplitudes are about the same order during a cycle. Thus the continuing existence of larger u_{rms} will result in the longer shear production and energy dissipation.

4. Conclusions

The linear stability of an oscillatory shear flow in a differentially heated vertical channel was investigated numerically. The parameters of $Re = 1000$ and $Pr = 0.7$ were used in these calculations. The results show that the least stable mode is the two-dimensional wave at low oscillation frequency and it tends to switch to three-dimensional disturbance at higher oscillation frequency. Generally, the critical value of $(Gr/Re)_c$ rapidly increases with the increasing oscillation frequency for the 2-D wave, and it gradually decreases with the increasing oscillation frequency for the 3-D disturbance. The flow oscillation acts to stabilize the flow at moderate and high oscillation frequencies except at low oscillation frequency.

The effect of oscillation amplitude shows a substantially different trend. For the oscillation amplitude, A, up to 0.3, all the least stable modes are dominated by 2-D waves at low oscillation frequency. Also, the flow oscillation acts to destabilize the flow and the amount of destabilization increases with the oscillation amplitude; but the least stable mode tends to become three-dimensional when the oscillation amplitude exceeds a threshold value at moderate and high oscillation frequencies. This threshold value is lower when the oscillation frequency is higher. Also, the flow oscillation acts to stabilize the flow and the degree of stabilization increases with the oscillation amplitude. All the critical wavenumbers for 2-D waves are very close to that (1.02) of Tollmien–Schlichting wave in the isothermal steady channel flow regardless of the oscillation amplitude and the oscillation frequency.

The instability type is the thermal-shear instability, where energy production by shear, E_s, is the driving mechanism for the flow instability. The characteristics of the E_s and the root mean square streamwise perturbation velocity, u_{rms}, are distinctively different between 2-D and 3-D disturbances. For the former, the peak value of u_{rms} is located near the hotter wall. The u_{rms} and E_s grow sharply when the base velocity begins to rise from its smallest value, and after reaching the peak value they decays rapidly during a short time interval, thus almost all the E_s is produced during only about 1/5 period of a cycle at low oscillation frequency. For the latter, the peak value of u_{rms} is located between channel center and cooler wall, where a wide range of the reverse flow exists near the cooler wall. The amplitudes of u_{rms}'s are large through the whole cycle, thus the E_s is generally generated during most of the time of a cycle.

Acknowledgements

The computing resource was provided by National Center for High-Performance Computing, Taiwan, R.O.C. The author is thankful to Mr. J.C. Lin for his work on code modification and the running of computer code.

References

[1] J.G. Zhang, U.H. Kurzweg, Numerical simulation of time-dependent heat transfer in oscillatory pipe flow, J. Thermophys. 5 (1991) 401–406.
[2] U.H. Kurzweg, Enhanced heat conduction in oscillating viscous flows within paralell-plate channels, J. Fluid Mech. 156 (1985) 291–300.
[3] U.H. Kurzweg, L.D. Zhao, Heat transfer by high frequency oscillations: a new hydrodynamic technique for achieving large effective thermal conductivities, Phys. Fluids 27 (1984) 2624.
[4] M. Kaviany, Performance of a heat exchanger based on enhanced heat diffusion in fluids by oscillation: analysis, ASME J. Heat Transfer 112 (1990) 49–55.
[5] M. Kaviany, M. Reckker, Performance of a heat exchanger based on enhanced heat diffusion in fluids by oscillation: experiment, ASME J. Heat Transfer 112 (1990) 56–63.
[6] Q.D. Liao, K.T. Yang, V.W. Nee, An analysis of conjugate heat transfer from a heated wall in a channel with zero-mean oscillatory flow for small oscillatory flow Reynolds

numbers, Int. J. Heat Mass Transfer 37 (Suppl.) (1994) 415–423.
[7] M. Faghri, K. Javdani, A. Faghri, Heat transfer with laminar pulsating flow in a pipe, Lett. Heat Mass Transfer 6 (1979) 259–270.
[8] N.J. Rabadi, J.C.F. Chow, H.A. Simon, Heat transfer in curved tubes with pulsating flow, Int. J. Heat Mass Transfer 25 (1982) 195–203.
[9] C.E. Grosch, H. Salwen, The stability of steady and time dependent plane Poiseuille flow, J. Fluid Mech. 34 (1968) 177–205.
[10] C. Von Kerczek, The instability of oscillatory plane Poiseuille flow, J. Fluid Mech. 116 (1982) 91–114.
[11] B.A. Singer, J.H. Ferziger, H.L. Reed, Numerical simulation of transition in oscillatory plane channel flow, J. Fluid Mech. 208 (1989) 45–66.
[12] R.G. Finucane, R.E. Kelly, Onset of instability in a fluid layer heated sinusoidally from below, Int. J. Heat Mass Transfer 19 (1976) 71–85.
[13] R.E. Kelly, H.-C. Hu, The onset of Rayleigh–Benard convection in non-planar oscillatory flows, J. Fluid Mech. 249 (1993) 373–390.
[14] R.E. Kelly, Stabilization of Rayleigh–Benard convection by means of slow nonplanar oscillatory flow, Phys. Fluids 4 (1992) 647–648.
[15] A.C. Or, R.E. Kelly, Onset of Marangoni convection in a layer of fluid modulated by a weak nonplanar oscillatory shear, Int. J. Heat Mass Transfer 38 (1995) 2269–2279.
[16] Y.C. Chen, J.N. Chung, Stability of mixed convection in a differentially heated vertical channel, ASME J. Heat Transfer 120 (1998) 127–132.
[17] Y.C. Chen, J.N. Chung, A direct numerical simulation of K- and H-type flow transition in a heated vertical channel, Phys. Fluids 14 (2002) 3327–3346.
[18] Y.C. Chen, J.N. Chung, A direct numerical simulation of transition phenomena in a mixed convection channel flow, Comput. Fluids 32 (2003) 795–822.
[19] J.E. Hart, Stability of the flow in a differentially heated inclined box, J. Fluid Mech. 47 (1971) 547–576.
[20] Y.C. Chen, J.N. Chung, The linear stability of mixed convection in a vertical channel flow, J. Fluid Mech. 325 (1996) 29–51.
[21] D. Gottlieb, S.A. Orszag, Numerical analysis of spectral methods: theory and applications. Society for Industrial and Applied Mathematics, Phil., PA, 1981.
[22] Y.C. Chen, J.N. Chung, The linear stability of an oscillatory two-phase channel flow in the limit of small Stokes numbers, Phys. Fluids 7 (1995) 1510–1512.
[23] S.A. Orszag, Accurate solution of the Orr–Sommerfeld stability equation, J. Fluid Mech. 50 (1971) 689–703.